Progress In Electromagnetics Research, PIER 39, 93–123, 2003

AN EFFECTIVE POWER SYNTHESIS TECHNIQUE FOR SHAPED, DOUBLE-REFLECTOR MULTIFEED ANTENNAS

O. M. Bucci, A. Capozzoli, and G. D'Elia

Dipartimento di Ingegneria Elettronica e delle Telecomunicazioni
Università di Napoli "Frederico II"
Via Claudio, 21, 80125 Napoli, Italy

Abstract—A new synthesis algorithm for shaped, double-reflector antennas with complex array feed is presented.

The approach presented here aims to improve the efficiency of synthesis techniques without missing the required accuracy. The algorithm is based on a convenient splitting of the original problem into two phases, each one involving a sub-problem significantly simpler than the original one.

A double reflector synthesis problem involving only Fourier Transform (FT) operators is of concern during the first phase. The subreflector surface and a first estimate of the main reflector geometry are obtained in this step. A single reflector synthesis problem is considered during the second phase wherein the final main reflector surface and the excitation coefficients of the primary feed array are obtained. While in the first phase only approximate relationships between the unknowns and the secondary radiated field are exploited, in the second phase accurate radiation operators are involved. Despite this accuracy, the second phase is still numerically effective since it involves a single reflector synthesis problem and exploits, as "good" starting point, the main reflector estimate obtained during the first phase.

The effectiveness of the approach is due to the fact that the necessity of dealing simultaneously with two reflector surfaces, the key of the synthesis difficulties, is afforded only during the first phase where efficient computational tools are allowed.

A numerical example shows the effectiveness of the proposed approach.

1. INTRODUCTION

Dual reflector antenna systems are exploited in radio astronomy, telecommunications or radar applications to meet stringent design requirements. Such systems are of interest also for special applications, such as compact range antennas [1], feeding structures for very large radio telescopes [2, 3], reconfigurable reflectors [4, 5]. During the years, a large number of dual reflector synthesis techniques have been introduced in order to design reflector geometries and feeding structures allowing to satisfy "at the best" the far-field pattern requirements.

The approaches available for reflector shaping are essentially of two types: (GO) and (PO) based ones. A useful set of references on these techniques and a brief critical discussion on the topic can be found in [6].

Here we only stress that GO shaping can be exploited to synthesize either the far-field pattern [7] or the main reflector aperture field, suitably obtained from the desired far-field pattern (e.g., by an optimization technique [8]). These techniques do not incorporate diffraction effects so that, the radiation pattern of the synthesized antenna usually differs significantly from the specified pattern. Furthermore, only a single element primary feed can be handled.

PO based approaches avoid these drawbacks and are based on the optimization of an objective functional accounting for the "distance" between the required and the synthesized pattern [9]. Various techniques have been proposed in order to make the PO approach numerically effective as, f.i., the successive projection algorithm [10] or the heuristic gradient based iterative procedure presented in [11].

A rigorous iterative synthesis algorithm based on the so called generalized projections has been presented in [12]. It can deal with an arbitrary antenna fed by a complex feeding array, and with far-field pattern requirements expressed in a completely general and flexible way by means of upper and lower bounds on the squared amplitudes of the far-field components. Although it has been applied to a single reflector antenna (multi beams or reconfigurable beams shaped reflector antennas with phase only control are considered in [13]), this approach can be exploited also for shaped double-reflector antennas. In particular, it allows synthesizing both the reflector surfaces and the feed array excitations.

A general PO based synthesis algorithm, exploiting "the antenna characterization and parameters optimization" concept, has been presented in [6]. As in [12], the reflector surfaces and the primary feed excitation coefficients represent the parameters to be found by an optimization process wherein the far-field pattern specifications are given by prescribing the values of the far-field pattern at given observation directions. The surface and the contour of the reflector are represented by modified Jacobi polynomials and a superquartic function, respectively, allowing to effectively manage the geometry of the problem [6]. The general approach, based on a standard Newton local optimization scheme, has been applied to a few examples of practical interest [6].

However, the accuracy of the electromagnetic model exploited by such a technique requires large computing time and/or memory, particularly in the case of electrically large reflectors. Accordingly, as referred in [6], despite the continuous grow of the computing resources, new advanced synthesis strategies with improved computational efficiency are still of interest.

Moreover, to fully exploit all the degrees of freedom in the structure to be synthesized, advanced optimization techniques could be exploited [6,14]. However, due to the high computational complexity of Global Optimization techniques, the practical and reliable application of such strategies requires a ticklish balance between the accuracy of the model and the computational efficiency.

It must be stressed that the computational heaviness of a PO based synthesis mainly rises from the need of a simultaneous deter-

mination of the surfaces of both reflectors. In fact, each step of the iterative procedures requires the evaluation of couples of PO double integrals for gradient and/or far-field computation.

To circumvent this drawback, a hybrid approach exploiting the PO and GO for the main and subreflector analysis, respectively, has been recently presented in [15] by suitably modifying the technique presented in [6]. However, in this case, since the subreflector diffraction effects are neglected, the compromise between accuracy and computational effectiveness can result unsatisfactory from the accuracy point of view.

Aim of this paper is to introduce a new double-reflector antenna power synthesis technique, based on the Aperture Method (AM) and PO for the analysis of the main reflector and of the subreflector, respectively, which achieve both computational efficiency and accuracy. The approach exploits the advanced minimization scheme presented in [12] to synthesize the main and sub-reflector geometries as well as the primary feed excitations. It attains efficiency by conveniently splitting the synthesis procedure into two phases, each one involving a sub-problem simpler than the original one.

During the first phase, the subreflector geometry and a first rough estimate of the main reflector surface are obtained. The approximations of the electromagnetic model involved in this first step allow a FT relationship between the unknowns and the secondary far-field. Accordingly, the FFT algorithm can be exploited to significantly reduce the numerical effort. During this phase the feeding structure is accounted for by only exploiting information on its location and size.

During the second phase, the above approximations are removed by performing the main and subreflector analysis by means of the AM and PO techniques, respectively. The final main reflector surface and the primary feed excitation coefficients are then found. The computational complexity of this second phase is strongly reduced with respect to the original double-reflector synthesis problem, since it simply involves a single (unknown) reflector. Furthermore, the result of the first phase of the procedure provides a good starting point for the main reflector surface, which is crucial to avoid trapping problems [12].

Accordingly, the effectiveness of the approach relies on the fact that the simultaneous determination of the two reflector surfaces, the heaviest part of the synthesis problem, is attained by exploiting the FFT, while the accurate input-output operators are involved only in a single reflector synthesis problem.

At variance of the approach presented in [15], main and subreflector diffraction effects are accounted for in both phases, approximately

in the first one and accurately during the second one that only corrects for the previously introduced approximations.

The statement of the problem and the solution strategy is discussed in Section 2.

The splitting of the original problem into simpler sub-problems and the two phases of the synthesis algorithm are presented in Section 3.

The discussion on the well position of the problem and the iterative synthesis algorithm are presented in Section 4.

The main results of a numerical analysis are shown in Section 5 while the final conclusions are drawn in Section 6.

2. STATEMENT OF THE PROBLEM AND SOLUTION STRATEGY

As mentioned in the Introduction, the aim of this paper is to present a new power pattern synthesis technique for double-reflector antennas able to effectively face the difficulties related to the simultaneous determination of the main reflector and subreflector surfaces as well as feed excitations.

With reference to Fig. 1, let us consider two centred reflectors and a planar feed array of N_F elementary radiators, located at (x_{F_i}, y_{F_i}), $i = 1, \ldots, N_F$.

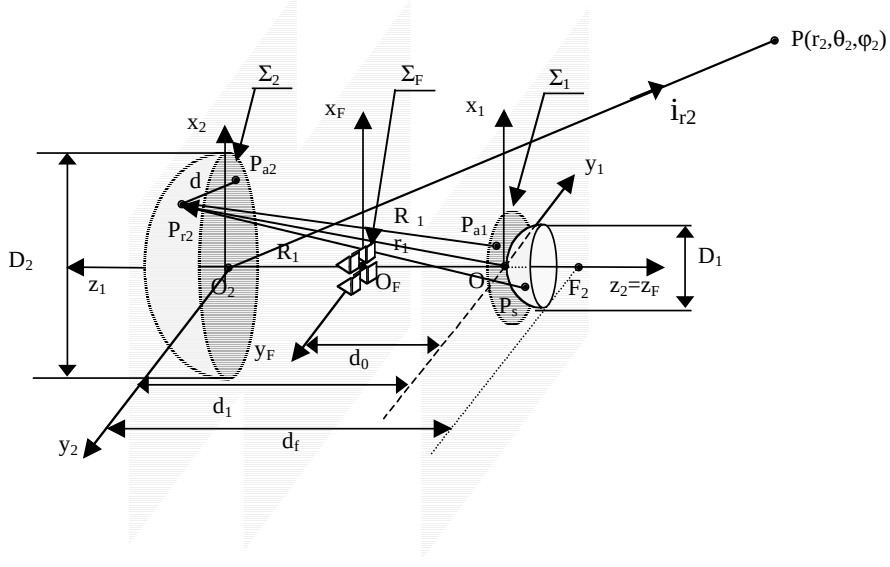

Figure 1. Geometry of the problem.

Denote with $\Sigma_F, \Sigma_1, \Sigma_2$ and D_F, D_1, D_2 the feed, secondary and main reflector apertures and diameters, respectively, with $S_F(O_F, x_F, y_F, z_F)$, $S_1(O_1, x_1, y_1, z_1)$ and $S_2(O_2, x_2, y_2, z_2)$ three, z-aligned, reference systems such that $O_F \in \Sigma_F$, $O_1 \in \Sigma_1$, $O_2 \in \Sigma_2$, $\hat{i}_{x1} = \hat{i}_{x2} = \hat{i}_{xF}$, $-\hat{i}_{y1} = \hat{i}_{y2} = \hat{i}_{yF}$, $-\hat{i}_{z1} = \hat{i}_{z2} = \hat{i}_{zF}$, and with d_0 and d_1 the distances $\overline{O_1O_F}$ and $\overline{O_2O_1}$, respectively. Moreover assume and drop the $e^{j\omega t}$ dependence and denote with λ the wavelength and $\beta = 2\pi/\lambda$.

Let $z_2 = g_2(x_2, y_2)$ and $z_1 = g_1(x_1, y_1)$ be the equations of the primary and secondary reflecting surfaces with respect to S_2, and S_1, respectively, $(r_2, \vartheta_2, \varphi_2)$ the spherical coordinates (within S_2) of a given observation point, $u_2 = \sin\vartheta_2 \cos\varphi_2$, $v_2 = \sin\vartheta_2 \sin\varphi_2$, $\underline{E}(r_2, u_2, v_2)$ the radiated field, $E_{co}(u_2, v_2)$ and $E_{cr}(u_2, v_2)$ the far-field co-polar and cross-polar patterns defined as $(E_{co}(u_2, v_2), E_{cr}(u_2, v_2)) = \lim_{r_2 \to \infty} [(\lambda r_2/j)\exp(j\beta r_2)\underline{E}(r_2, u_2, v_2)]$ and $\underline{C} = (C_1, \ldots, C_{N_F})$ the vector of the excitation coefficients of the feed radiators.

For the sake of generality, we will assume that the far-field pattern specifications refer to a bounded observation domain of the (u, v) plane, say Ω, and that they are prescribed by means of two co-polar and cross-polar "masks", within which $|E_{co}|^2$ and $|E_{cr}|^2$ should lie and whose upper and lower bounds are given by the functions M_{co}, M_{cr} and m_{co}, m_{cr}, respectively, defined on Ω.

Under the natural assumption that the overall antenna dimensions and the primary feed array are given, i.e., that D_1, D_2, D_F, d_0, d_1, N_F, $(x_{F_i}, y_{F_i})_{i=1,\ldots,N_F}$ are known, the goal of the synthesis procedure is to determine g_1, g_2 and $\underline{C}$ to meet the design specifications expressed by means of M_{co}, M_{cr}, m_{co}, m_{cr}.

As stated in the Introduction, we apply the AM for evaluating the far-field of the main reflector. This increases the computational efficiency of the approach, while being practically equivalent to the PO from the accuracy point of view [16], provided that the aperture caps the (concave) reflector. On the contrary, the PO approximation is applied to evaluate the field scattered by the subreflector. Accordingly $E_{co}(u_2, v_2)$ and $E_{cr}(u_2, v_2)$ are given by:

$$\begin{aligned}(E_{co}, E_{cr}) &= A_1 \underline{\underline{Q}}(u_2, v_2) \iint_{\Sigma_2} \underline{E}^t_{a2}(\xi_2, \eta_2) e^{j2\pi(\xi_2 u_2 + \eta_2 v_2)} d\xi_2 d\eta_2 \\ &= A \underline{\underline{Q}} \mathcal{F}^{-1} \lfloor P_{\Sigma_2} \underline{E}^t_{a2} \rfloor \end{aligned} \tag{1}$$

where $\mathcal{F}$ is the Fourier Transform (FT) operator, P_{Σ_2} is the characteristic function associated to the domain Σ_2, A_1 is an unessential dimensional constant, $(\xi_2 = x_2/\lambda,\ \eta_2 = y_2/\lambda, 0)$ are the normalised co-ordinates of a point, say P_{a2}, of Σ_2, $\underline{E}^t_{a2}(\xi_2, \eta_2)$ is the transverse (to $\hat{i}_{z2}$) component of the aperture field at P_{a2}, and $\underline{\underline{Q}}$ is the matrix

transforming the transverse components of the spectrum into the co-polar and cross-polar components of the far-field pattern.

In the frame of the AM, the aperture field $\underline{E}_{a2}(\xi_2, \eta_2)$ at P_{a2} is due to the contributions of all rays (evaluated according to laws of GO) stemming from the subreflector surface and passing through P_{a2} after reflection on the main reflector surface†.

Accordingly, $\underline{E}_{a2}(\xi_2, \eta_2)$ is given by‡:

$$\underline{E}_{a2}(\xi_2, \eta_2) = A_2 \iint_{\Sigma_1} e^{-j\beta(R_1+d)} \frac{\Delta}{R_1} \underline{\underline{R}}(\underline{\underline{I}} - \underline{\hat{R}}_1 \underline{\hat{R}}_1) \underline{J}_1 d\xi_1 d\eta_1 \qquad (2)$$

wherein (see Fig. 1) A_2 is an unessential dimensional constant, $\underline{\underline{R}}$ is the reflection matrix at the reflection point P_{r2}, $d = \overline{P_{a2}P_{r2}}$,

$$\Delta = \sqrt{\frac{\rho_1 \rho_2}{(\rho_1 + d)(\rho_2 + d)}} \qquad (3)$$

is the divergence factor of the reflected pencil with principal radii of curvature equal to ρ_1 and ρ_2,

$$\underline{J}_1(\xi_1, \eta_1) = \left[\frac{\partial g_1}{\partial \xi_1 \partial \eta_1} \right] 2\hat{i}_{n_1} \times \underline{H}_i(\underline{C}, \xi_1, \eta_1, g_1(\xi_1, \eta_1)) \qquad (4)$$

is the equivalent current induced (in the PO approximation) by the primary field at the generic subreflector point P_S, with normalised coordinates $\xi_1 = x_1/\lambda$, $\eta_1 = y_1/\lambda$, $\zeta_1 = g_1(x_1, y_1)/\lambda)$, $\underline{R}_1 = R_1 \hat{R}_1 = P_{r2} - P_s$, $\hat{i}_{n1}$ the unit vector normal to the subreflector at P_s and $\underline{H}_i$ the magnetic field incident on the subreflector surface at P_s, linearly related to the excitation vector $\underline{C}$.

It is worth noting that, apart from $\underline{J}_1$, all the terms appearing in the integral of eq. (2) depend on $(\xi_1, \eta_1, \xi_2, \eta_2)$.

From eqs. (1)–(4), we get:

$$\begin{aligned}(E_{co}, E_{cr}) \; = \; & \underline{\underline{Q}} \cdot \mathcal{F}^{-1} \Bigg\{ P_{\Sigma_2} \hat{i}_{z2} \times \Bigg[\iint_{\Sigma_1} e^{-j\beta(R_1+d)} \frac{\Delta}{R_1} \underline{\underline{R}}(\underline{\underline{I}} - \underline{\hat{R}}_1 \underline{\hat{R}}_1) \\ & \cdot \left[\frac{\partial g_1}{\partial \xi_1 \partial \eta_1} \right] 2\hat{i}_{n_1} \times \underline{H}_i(\underline{C}, \xi_1, \eta_1, g_1(\xi_1, \eta_1)) d\xi_1 d\eta_1 \Bigg] \times \hat{i}_{z2} \Bigg\} \qquad (5)\end{aligned}$$

where the unessential constants A_1 and A_2 have been incorporated within the unknown excitation coefficients appearing in the expression of $\underline{H}_i$.

† A single reflection point is assumed in the following.

‡ Obviously, it is assumed that $R_1 \gg \lambda$.

Eq. (5) clearly shows the difficulties encountered when facing the double reflector synthesis problem. First, the relationship between (E_{co}, E_{cr}) and the unknowns is non-linear and very complex, and involves the exponential terms, the Jacobians of the reflectors equation, the reflectors normal and the incident magnetic primary field. Second, due to this dependence and to the double integrals, the evaluation of the secondary pattern is very expensive from the computing time and/or memory storage requirement point of view.

These difficulties make unpractical the application of a standard AM-PO based synthesis algorithm: the complexity of the problem asks for an iterative optimisation procedure, requiring the repeated evaluation of the secondary pattern[§].

A possible way to get an effective double-reflector antenna synthesis, is to split the problem into simplest sub-problems, whose intermediate goals require smaller numerical efforts and involve simpler relationships between the unknowns and the intermediate outputs.

As addressed in the Introduction, we propose a two phases synthesis strategy. In the first phase, the subreflector geometry and a rough estimate of the main reflector surface are obtained by exploiting an approximate electromagnetic model of the radiating structure based on FT operators and a general description of the feed structure accounting for the available information on its aperture size and position. Then, in the second phase, the final main reflector surface and the primary feed excitations are obtained by exploiting the more complex and accurate AM-PO operators as well as by explicitly taking into account the primary feeding structure.

Following this approach, the two reflecting surfaces must be simultaneously taken into account only during the first phase, where a numerically efficient FFT algorithm can be exploited.

Also the second phase requires a significantly reduced computational effort, despite the complexity (and accuracy) of the involved radiation operators. In fact, only a single reflector synthesis problem is considered, i.e., a problem drastically less complex than the original one. Moreover, to solve this problem, a "good" starting point, i.e., the main reflector already obtained during the first phase, can be used with beneficial effects on the convergence rate as well as on the occurrence of trapping solutions.

As a matter of fact, the main step toward a satisfying solution of the synthesis problem is made during the first phase while the second one essentially corrects for the effects due to the approximations

[§] It must be noted that similar difficulties are encountered also in the case of a synthesis technique based on the PO approximation for the evaluation of the field scattered by the main reflector. In that case, even larger computational efforts would be required.

previously introduced. As such, it demands a reduced numerical effort.

3. THE TWO PHASES OF THE SYNTHESIS PROBLEM

In order to discuss the key points of the two phases and to introduce the corresponding approximations, let us consider in more detail the main reflector aperture field and the subreflector scattered field.

3.1. Main Reflector and Subreflector Aperture Field Factorization

With reference to the main reflector aperture field, let us analyze the effect on $\underline{E}_{a2}$ of a small, smooth variation of the main reflector geometry such that[‖]:

$$|\delta g_2| \ll D_2; \qquad |\nabla(\delta g_2)| \ll 1 \tag{6}$$

This implies that the variations of the geometrical factors appearing in the expression (2) for the aperture field can be neglected, leaving only to deal with the modification of the normalized optical path:

$$l_2 = \beta(R_1 + d) \tag{7}$$

due to the shift of the reflection point P_{r2}.

Evaluating the modification to the first order (see Appendix A) we get:

$$\delta l_2 = \delta l_2(P_{a2}, P_S) = 2\beta\chi\hat{i}_{n2} \cdot R_1 = 2\beta\chi\cos\alpha \tag{8}$$

being $\hat{i}_{n2}$ the normal versor at the (unperturbed) reflection point, χ the normal component of the deformation and α the angle between the reflected ray and $\hat{i}_{n2}$.

Exploiting relation (8) and Appendix B, the total variation of δl_2 as P_S moves inside a sphere enclosing the subreflector can be evaluated in the limiting cases of very large or zero surface curvature.

In the first case, the shifts of the reflection point can be neglected, and we get:

$$\nu(\delta l_2) = (\max_{P_S}(\delta l_2) - \min_{P_S}(\delta l_2)) = 4\beta\chi\sin(\alpha_0)\sin(\alpha_S) \tag{9a}$$

wherein α_0 is the semiangle between the reflected and the incident ray from the center, P_0, of the sphere and α_S the semiangle subtended by the sphere from P_{r2}.

[‖] The effects of the changes in the reflector curvatures are neglected.

In the second case, application of the images theorem immediately gives:

$$\nu(\delta l_2) = 4\beta\chi \sin(\alpha_0)\sin(\alpha_i) \tag{9b}$$

α_i being the semiangle subtended by the *image* of the sphere from P_{a2}.

Accordingly, as $\alpha_i \leq \alpha_S$, we get from (9a) and (9b):

$$\nu(\delta l_2) \leq 4\beta\chi \sin(\alpha_0)\sin(\alpha_S) \tag{10}$$

In the case of focusing antennas, it is natural to assume a parabolic dish with focus at P_0 as the reference (unperturbed) reflector. In this case (10) can be explicitly evaluated, and we get:

$$\max_{P_{a2}}(\nu(\delta l_2)) \lesssim \beta\chi \frac{D_1 D_2}{2f^2} \tag{11}$$

f being the focal distance of the paraboloid.

Relation (11) shows that even for relatively large values of aperture (D_2/f) and obstruction ratio (D_1/D_2), the difference $\delta l_2(P_{a2}, P_S) - \delta l_2(P_{a2}, P_0)$ can be safely neglected for deformations up to some wavelengths. Accordingly, the variations of $l_2(P_{a2}, P_S)$ can be assumed equal to those of $l_2(P_{a2}, P_0)$ and, for shaping not larger than some wavelength (with respect to the reference reflector), we can put:

$$l_2(P_{a2}, P_s) \cong \overline{l}_2(P_{a2}, P_s) + \delta l_2(P_{a2}, P_0) = \overline{l}_2(P_{a2}, P_s) + s_2(P_{a2}) \tag{12}$$

wherein $\overline{l}_2$ is the normalized optical path from P_s to P_{a2} relative to the reference reflector, and we get for the aperture field:

$$\underline{E}^t_{a2} = \underline{E}^t_{a20} e^{-j2\pi s_2} \tag{13}$$

being $\underline{E}^t_{a20}$ the transverse aperture field of the reference reflector.

Later on, for the sake of convenience, we will write $l_{20} = \overline{l}_2(P_{a2}, P_0)$ and $\underline{E}^t_{a2}(\xi_2, \eta_2) = \underline{F}_{a2}(\xi_2, \eta_2) e^{-j2\pi s_2(\xi_2,\eta_2)} e^{-j2\pi l_{20}(\xi_2,\eta_2)}$, where $\overline{l}_2(P_{a2}, P_0)$ is the (unperturbed) normalized optical path from the center of the sphere enclosing the subreflector.

The reference optical path l_{20} is useful if one aims to force the reflector to be close enough to a given surface. Furthermore, since the radiated far-field intensity depends on the optical path but for an additive constant (that modifies the resulting reflector geometry), it introduces a useful degree of freedom in the reflector surface determination [13].

It is stressed that, within the approximations previously considered, the factor $\underline{F}_{a2}(\xi_2, \eta_2)$ has a weak dependence on the main reflector distortions (i.e., s_2) so that the dependence of the secondary scattered

field on the main reflector surface essentially reduces to the exponential term $e^{-j2\pi s_2}$.

As far as the subreflector aperture field $\underline{E}_{a1}$ is concerned, similar considerations can be applied. In particular, the transverse component (to $\hat{i}_{z1}$) of $\underline{E}_{a1}$, say $\underline{E}^t_{a1}$, can be written as:

$$\underline{E}^t_{a1}(\xi_1,\eta_1) = e^{-j2\pi l_{10}(\xi_1,\eta_1)} e^{-j2\pi s_1(\xi_1,\eta_1)} \underline{F}_{a1}(\xi_1,\eta_1) \tag{14}$$

where l_{10}, l_1 and s_1 have the same meaning than l_{20}, l_2 and s_2 but refer now to the subreflector surface, to a reference subreflector and to the centre of the sphere enclosing the feeding system. Again $\underline{F}_{a1}$ can be assumed essentially independent on s_1 so that the dependence of $\underline{E}^t_{a1}$ on the subreflector surface, i.e., on g_1, simplifies and is confined to the exponential term $e^{-j2\pi s_1}$.

However, something more can be said on $\underline{F}_{a1}$. In fact, it can be shown [13] that $\underline{F}_{a1}$ is an essentially band limited function of the variables (ξ_1,η_1) with a bandwidth, say w_s, given by $w_s = 2\pi D_1/d_0$.

As a consequence, we get:

$$\underline{F}_{a1}(\xi_1,\eta_1) = \mathcal{F}\lfloor P_{w_s}(\kappa,\nu)\underline{F}_{a0}(\kappa,\nu)\rfloor \tag{15}$$

where (κ,ν) are the variables conjugate (through the FT) to (ξ_1,η_1), P_{w_s} is the characteristic function of the domain $\Xi = \{(\kappa,\nu) : \sqrt{\kappa^2+\nu^2} \le w_s\}$ and the unknown function $\underline{F}_{a0}$ is an unknown vector function, assumed square integrable on Ξ.

3.2. Splitting the Synthesis Problem

The above factorisations are useful to find an approximate relationship between the far-field copolar and crosspolar components and the unknowns of the problem. In particular, it is convenient to express the primary scattered field by exploiting the AM. For points at least some wavelength far from the subreflector aperture, we have, apart from an unessential dimensional constant A_3:

$$\underline{E}_S = A_3 \iint_{\Sigma_{e1}} \frac{e^{-j\beta R'_1}}{R'_1} \hat{i}_{R'_1} \times [\hat{i}_{z1} \times \underline{E}_{a1}] d\xi_1 d\eta_1 \tag{16}$$

where Σ_{e1} is the subreflector (enlarged) aperture involved in the application of the AM, $(\xi_1 = x_1/\lambda,\ \eta_1 = y_1/\lambda, 0)$ are the normalised coordinates (within the reference system S_1) of P_{a1} and $R'_1 = P_{r2} - P_{a1}$ is the vector joining the equivalent source point to the observation point (see Fig. 1).

Accordingly, by grouping the unessential constant in a dimensional constant A_4, the secondary aperture field $\underline{E}_{a2}$ can be expressed as:

$$\underline{E}_{a2} = A_4 \iint_{\Sigma_{e1}} e^{-j\beta(R_1'+d)} \frac{\Delta}{R_1'} \underline{\underline{R}}\, \hat{i}_{R_1'} \times [\hat{i}_{z1} \times \underline{E}_{a1}] d\xi_1 d\eta_1 \tag{17}$$

Taking into account the main reflector and subreflector aperture field factorization (13) and (14), respectively, we obtain:

$$\begin{aligned} \underline{E}_{a2}^t &= \underline{F}_{a2} e^{-j2\pi l_{20}} e^{-j2\pi s_2} \\ &= A_4 \hat{i}_{z1} \times \iint_{\Sigma_{e1}} e^{-j\beta(R_1'+d)} \frac{\Delta}{R_1'} \underline{\underline{R}} \cdot \hat{i}_{R_1'} \\ &\quad \times [\hat{i}_{z1} \times \underline{F}_{a1} e^{-j2\pi l_{10}} e^{-j2\pi s_1}] d\xi_1 d\eta_1 \times \hat{i}_{z1} \end{aligned} \tag{18}$$

For reflector points located in the far-zone of the subreflector surface, exploiting the paraxial approximation [17], eq. (18) reduces to:

$$\begin{aligned} \underline{F}_{a2}(\xi_2, \eta_2) &= A_4 \frac{1}{d_1} \iint_{\Sigma_{e1}} e^{j2\pi \frac{\xi_1\xi_2 + \eta_1\eta_2}{d_1}} \\ &\quad \cdot e^{-j2\pi l_{10}(\xi_1,\eta_1)} e^{-j2\pi s_1(\xi_1,\eta_1)} \underline{F}_{a1}(\xi_1, \eta_1) d\xi_1 d\eta_1 \end{aligned} \tag{19}$$

Finally, from eqs. (1), (13), (15) and (19), we obtain:

$$\begin{aligned} &(E_{co}(u_2, v_2), E_{cr}(u_2, v_2)) \\ &\quad = \mathcal{L}(s_1, s_2, \underline{F}_{a0}) \\ &\quad = (\mathcal{L}_{co}(s_1, s_2, \underline{F}_{a0}), \mathcal{L}_{cr}(s_1, s_2, \underline{F}_{a0})) \\ &\quad = \underline{\underline{Q}} \mathcal{F}^{-1} \Big\{ P_{\Sigma_2} e^{-j2\pi l_{20}} e^{-j2\pi s_2} \\ &\qquad \cdot \mathcal{F}^{-1} \left[P_{\Sigma_{e1}} e^{-j2\pi l_{10}} e^{-j2\pi s_1} \left(\mathcal{F}(P_w \underline{F}_{a0}(\kappa, \nu)) \right) \right] \Big\} \end{aligned} \tag{20}$$

where all unessential constants have been incorporated within the unknown dimensional function $\underline{F}_{a0}$, $P_{\Sigma_{e1}}$ is the characteristic function of Σ_{e1} and the functional dependence between the radiated pattern and the unknowns is represented by the operator $\mathcal{L}$.

Eq. (20) expresses the well-known property: within the paraxial approximation, the double-reflector antenna essentially behaves as a couple of lenses. It allows a simple description of the main effects of the reflector surfaces on the radiated fields as well as it simply incorporates some relevant information on the geometry of the primary feed.

As such, it will represent the basic relationship exploited in the first phase of the synthesis, wherein s_1, s_2, and F_{a0} are assumed as intermediate unknowns.

Once the values of s_1 and s_2 are obtained, say s_{10} and s_{20}, the subreflector surface and a first estimate of the main reflector, say g_{10} and g_{20}, can then be obtained by simple geometrical considerations [18, 13]. In fact, for a fixed reference surface, there is a one to one correspondence between the function $g(x, y)$ describing the reflector surface $z = g(x, y)$ and the optical path difference $s(x, y)$. In other words, we can write $g = \mathcal{W}(s)$ being $\mathcal{W}$ a suitable operator. In particular, we have $g_{10} = \mathcal{W}(s_{10})$ and $g_{20} = \mathcal{W}(s_{20})$.

Taking into account these relationships and the linear dependence of the primary incident field $\underline{H}_i$ on the feed excitation coefficients $\underline{C}$, eq. (5), can be reassessed as:

$$\begin{aligned}
&(E_{co}(u_2, v_2), E_{cr}(u_2, v_2)) \\
&\quad = \mathcal{J}(s_1, s_2, \underline{C}) \\
&\quad = (\mathcal{J}_{co}(s_1, s_2, \underline{C}), \mathcal{J}_{cr}(s_1, s_2, \underline{C})) \\
&\quad = \underline{\underline{Q}}\mathcal{F}^{-1}\Bigg\{ P_{\Sigma_2}\hat{i}_{z2} \times \Bigg[\iint_{\Sigma_1} e^{-j\beta(R_1+d)} \frac{\Delta}{R_1} \underline{\underline{R}} \cdot (\underline{\underline{I}} - \hat{R}_1\hat{R}_1) \\
&\qquad \cdot \left[\frac{\partial \mathcal{W}(s_1)}{\partial \xi_1 \partial \eta_1} \right] 2\hat{i}_{n_1} \times \sum_{n=1}^{N_F} C_n \underline{H}_{in} d\xi_1 d\eta_1 \Bigg] \times \hat{i}_{z_2} \Bigg\}
\end{aligned} \tag{21}$$

where $\underline{H}_{in}$ is the contribution of the n-th elementary radiator to the magnetic field incident on the subreflector surface and the functional dependence between the radiated pattern and the unknowns is represented by the operator $\mathcal{J}$.

As previously stated, during the second stage of the synthesis procedure, the subreflector surface will be assumed unchanged and the relationship (21) will be exploited with $g_1 = g_{10}$. In particular, assuming as a starting main reflector the surface defined by the equation $z = g_{20} = \mathcal{W}(s_{20})$, the main reflector surface, hence s_2, and the primary feed excitation coefficients, hence $\underline{C}$, will be found in order to satisfy the design specifications expressed by means of M_{co}, M_{cr}, m_{co}, and m_{cr}.

In the practical application of the technique, the optical paths s_1 and s_2 have been represented as a series of a finite number of Tchebytchev polynomials (see Appendix C).

Accordingly, the determination of the expansion coefficients (together with the excitation vector $\underline{C}$) becomes the goal of the synthesis technique.

Details on the adopted representations and the expressions of the radiated field exploited in both phases and corresponding to eqs. (20), (21), are given in the Appendix C.

4. THE SYNTHESIS ALGORITHM

Now let us give a detailed description of the two phases of the synthesis procedure.

In the first phase, wherein s_1, s_2, and $\underline{F}_{a0}$ are found by exploiting eq. (20), we assume $\underline{F}_{a0} \in \mathbf{L}_2(\Xi) \times \mathbf{L}_2(\Xi)$, where $\mathbf{L}_2(\Xi)$ denotes the space of square integrable functions over Ξ.

First, the well position and well conditioning of the problem is considered.

In fact, as discussed in [12], the problem is ill posed or, at least, ill conditioned since the region Ω of interest is bounded.

Following [12], the regularisation can be obtained by controlling the power of the co-polar and cross-polar pattern outside Ω and by keeping it as small as possible.

Later on, this goal is attained by introducing the sets:

$$\mathbf{Y}_{co} : \Big\{ y \in \mathbf{L}_2 \text{ and } y \geq 0 : \left\{ \begin{array}{ll} m_{co}(u,v) \leq y(u,v) \leq M_{co}(u,v) & \text{when } (u,v) \in \Omega \\ 0 & \text{when } (u,v) \notin \Omega \end{array} \right\} \tag{22}$$

$$\mathbf{Y}_{cr} : \Big\{ y \in \mathbf{L}_2 \text{ and } y \geq 0 : \left\{ \begin{array}{ll} m_{cr}(u,v) \leq y(u,v) \leq M_{cr}(u,v) & \text{when } (u,v) \in \Omega \\ 0 & \text{when } (u,v) \notin \Omega \end{array} \right\} \tag{23}$$

and by finding s_1, s_2, and $\underline{F}_{a0}$ such that $|\mathcal{L}_{co}(s_1, s_2, \underline{F}_{a0}|^2$ and $|\mathcal{L}_{cr}(s_1, s_2, \underline{F}_{a0})|^2$ are as close as possible to $\mathbf{Y}_{co}$ and $\mathbf{Y}_{cr}$, respectively.

Furthermore we introduce a constraint on the subreflector aperture field to control the antenna gain. In particular we require that the power content of $\underline{F}_{a1}$ outside Σ_{e1} is as small as possible (with additional beneficial effects on the well conditioning of the problem).

Finally, a physical constraint on $s_1 = l_1 - l_{01}$ and $s_2 = l_2 - l_{02}$ must be enforced to make possible the calculation of g_1 and g_2 by GO [18]. In fact, l_1 and l_2 are optical paths and they must satisfy the eikonal equation:

$$|\nabla_t l_2|^2 = |\nabla_t (l_{20} + s_2)|^2 \leq 1 \tag{24a}$$

$$|\nabla_t l_1|^2 = |\nabla_t (l_{10} + s_1)|^2 \leq 1 \tag{24b}$$

where ∇_t represents the "nabla" operator with respect to the variables transverse to the z axis.

Equivalently, $\nabla_t(l_{10}+s_1)$ and $\nabla_t(l_{20}+s_2)$, as elements of the space of square integrable functions, must belong to the unit sphere, say $\mathbf{S}_\infty$, in the uniform norm.

This is a tight constraint so that a constrained searching of the unknowns $s_1,\ s_2$, and $\underline{F}_{a0}$ should be performed. However, the related difficulties suggested an unconstrained searching procedure considering a suitable additive terms in the objective functional. Accordingly, $s_1,\ s_2$, and $\underline{F}_{a0}$ have been obtained by minimising the functional:

$$\begin{aligned}\Gamma_1(s_1, s_2, \underline{F}_{a0}) = & \\ & \left\| |\mathcal{L}_{co}(s_1, s_2, \underline{F}_{a0})|^2 - \mathcal{P}_{\boldsymbol{Y}_{co}} |\mathcal{L}_{co}(s_1, s_2, \underline{F}_{a0})|^2 \right\|_{w_{co}}^2 \\ & + \left\| |\mathcal{L}_{cr}(s_1, s_2, \underline{F}_{a0})|^2 - \mathcal{P}_{\boldsymbol{Y}_{cr}} |\mathcal{L}_{cr}(s_1, s_2, \underline{F}_{a0})|^2 \right\|_{w_{cr}}^2 \\ & + \gamma_1 \left\| P_{\Sigma_1} |\nabla_t (l_{10} + s_1)|^2 - \mathcal{P}_{S_\infty} P_{\Sigma_1} |\nabla_t (l_{10} + s_1)|^2 \right\|_1^2 \\ & + \gamma_2 \left\| P_{\Sigma_2} |\nabla_t (l_{20} + s_2)|^2 - \mathcal{P}_{S_\infty} P_{\Sigma_2} |\nabla_t (l_{20} + s_2)|^2 \right\|_1^2 \\ & + \gamma_3 \left\| (1 - P_{\Sigma_{e1}}) |\mathcal{F}(P_{w_s} \underline{F}_{a0})|^2 \right\|_1^2 \end{aligned} \tag{25}$$

where $\| \cdot \|_w$ represents the $\mathbf{L}_2$-norm referred to a properly defined weighting function w, $\gamma_1,\ \gamma_2$ and γ_3 are weighting factors, P_{Σ_1} is the characteristic function of Σ_1 and $\mathcal{P}_{\boldsymbol{Y}_{co}},\ \mathcal{P}_{\boldsymbol{Y}_{cr}},\ \mathcal{P}_{\boldsymbol{S}_\infty}$ are the metric projectors onto $\mathbf{Y}_{co},\ \mathbf{Y}_{cr}$ and $\mathbf{S}_\infty$, respectively.

The first two terms in (25) account for the distance of $|\mathcal{L}_{co}|^2$ and $|\mathcal{L}_{cr}|^2$ from $\mathbf{Y}_{co}$ and $\mathbf{Y}_{cr}$ respectively; the third and the fourth terms account for the eikonal constraint on s_1 and s_2, respectively; the fifth term controls the power content of the field on the subreflector aperture outside Σ_{e1}.

In this way the strict fulfilment of the eikonal equation for l_1 and l_2 must be verified *a posteriori* and, when not satisfied, the minimisation of Γ_1 must be repeated with increased values for γ_1 or γ_2 or both.

As previously outlined, once s_1 and s_2 are obtained, g_1 and g_2 are evaluated by exploiting a GO based technique [15, 13] leading to g_{10} and g_{20}.

Now the second phase starts.

During the second phase of the synthesis procedure the subreflector surface is assumed fixed and given by the equation $z_1 = g_{10}(x_1, y_1)$ while $\underline{C}$ and s_2 are assumed unknown in eq. (21) and are found to meet the far-field pattern design specifications expressed by $M_{co},\ M_{cr}$, and $m_{co},\ m_{cr}$.

Paralleling the previous discussion concerning the functional $\Gamma_1,\ \underline{C}$ and s_2 are obtained by minimising the objective functional:

$$\Gamma_2(s_2, \underline{C}) \ = \ \left\| |\mathcal{J}_{co}(s_{10}, s_2, \underline{C})|^2 - \mathcal{P}_{\boldsymbol{Y}_{co}} |\mathcal{J}_{co}(s_{10}, s_2, \underline{C})|^2 \right\|_{w_{co}}^2$$

$$+\left\| |\mathcal{J}_{cr}(s_{10}, s_2, \underline{C})|^2 - \mathcal{P}_{\boldsymbol{Y}_{cr}} |\mathcal{J}_{cr}(s_{10}, s_2, \underline{C})|^2 \right\|_{w_{cr}}^2$$
$$+\gamma_1 \left\| P_{\Sigma_2} |\nabla_t (l_{20} + s_2)|^2 - \mathcal{P}_{S_\infty} P_{\Sigma_2} |\nabla_t (l_{20} + s_2)|^2 \right\|_1^2$$
$$+\gamma_2 \left\| (1 - P_\Theta) |\underline{H}_i(\underline{C})|^2 \right\|_1^2 \tag{26}$$

where the last term controls the spillover of the primary feed power outside the subreflector angular sector (as seen from O_F), say Θ, and P_Θ is the characteristic function of Θ.

In the practical application of the technique, by exploring the adopted representation for s_1 and s_2, two functionals Φ_1 and Ψ_1 are minimized, as shown in Appendix C.

5. NUMERICAL ANALYSIS

In order to verify the effectiveness of the presented approach, the synthesis procedure has been implemented in a computer code and an extensive numerical analysis has been performed. Some significant results are reported in the following.

Aiming only to show the feasibility of the proposed synthesis technique, a simple centred double reflector antenna has been considered, simply accounting for the subreflector blockage effect by shadowing a circular dish of the main reflector aperture.

Two reflectors with $D_1 = 3\lambda$, $D_2 = 20\lambda$ and a primary feeding systems with five elementary Huygens radiators with co-ordinates $(0, 0)$, $(.5\lambda, 0)$, $(-.5\lambda, 0)$, $(0, .5\lambda)$, $(0, -.5\lambda)$, respectively (in the reference system S_F), have been considered. Referring to Fig. 1, we assumed $d_0 = 4.98\lambda$, $d_1 = 6.58\lambda$ and $d_f = 7.78\lambda$.

The copolar pattern specifications have been given by means of two masks made of two regions, the internal one with prescribed upper and lower levels equal to $+0.5\,\mathrm{dB}$ and $-0.5\,\mathrm{dB}$ and the external one with prescribed upper and lower levels equal to $-30\,\mathrm{dB}$ and $-200\,\mathrm{dB}$, respectively. The internal region is obtained from a coverage shape corresponding to the Italian peninsula and the Sicilia and Sardegna islands as seen from a point with 3200 km altitude and with latitude and longitude equal to 12° Est and 25° Nord, respectively. In particular the upper bound of the internal region is a version slightly enlarged of such coverage area while the lower bound of the internal region is a slightly restricted version of the same coverage.

An upper bound of $-70\,\mathrm{dB}$ has been required for the cross-polar component of the field.

During the first phase of the synthesis procedure we assumed as main reflector reference optical path the function $l_{20}(\xi_2, \eta_2) = c(\xi_2^2 +$

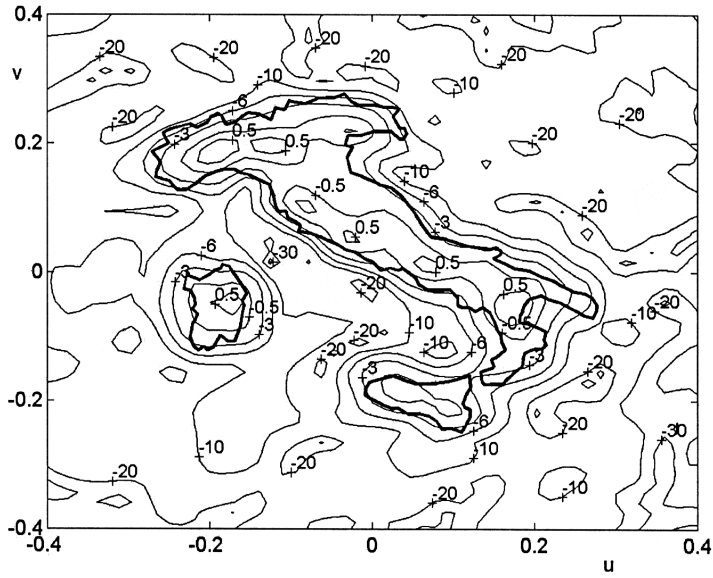

Figure 2. Copolar component synthesized during the first phase.

$\eta_2^2)/(D_2/\lambda)$ with $c = 0.3$ and as subreflector reference optical path the function $l_{10}(\xi_1, \eta_1) = \sqrt{\xi_1^2 + \eta_1^2 + (a_2 - a_1)^2} + 2a_1$, with $a_1 = 1.89$ and $a_2 = 3.09$, corresponding to a hyperbolic subreflector with focuses at points O_F and F_2 (see Fig. 1).

Then, the starting value of $\underline{F}_{a0}$ has been evaluated by inverting the operator $\mathcal{L}$ in eq. (20) and assuming that the co-polar component of the field is real and equal to the square root of the lower bound of the co-polar mask and that both the cross-polar component of the field and the starting values of s_1 and s_2 are equal to zero. Finally, the starting values of s_1 and s_2 have been assumed equal to the null functions.

During the second phase of the synthesis procedure, we assumed as starting main reflector optical path the one obtained from the first phase of the procedure while the starting excitations of the elementary radiators of the feed array have been set all equal to a constant.

The minimisation of the functionals Φ_1 and Ψ_1 introduced in the Appendix C (eqs. (C3) and (C7), respectively) has been performed by applying a quasi-Newton scheme, the BFGS (Broyden-Fletcher-Golfarb-Shanno) method with self scaling of the eigenvalues [19].

The co-polar and cross-polar components obtained at the first phase of the synthesis procedure are shown in Fig. 2 and Fig. 3,

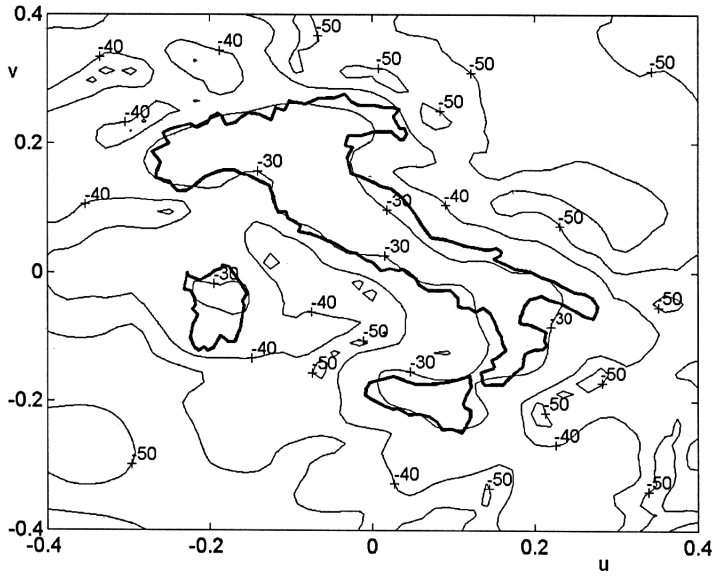

Figure 3. Crosspolar component synthesized during the first phase.

respectively, together with the considered coverage area. The synthesised subreflector and main reflector surfaces are shown in Fig. 4 and Fig. 5, respectively.

The co-polar and cross-polar components obtained during the second phase of the synthesis procedure are shown in Figs. 6 and 7, respectively. The final main reflector surface obtained during this phase is shown in Fig. 8. The amplitude and phases of the excitation coefficients of the five considered elementary sources are shown in Table 1.

In order to verify the reliability of these results and to validate the approach, the field radiated by the synthesised antenna has been independently evaluated by exploiting the physical optics approximation on both reflectors. The evaluated co-polar and cross-polar patterns, shown in Figs. 9 and 10, respectively, agree well with the results of the second phase of the presented synthesis procedure.

The behaviours of the objective functional during the first (eq. 20) and second phase (eq. 21) are shown under Figs. 11 and 12, respectively. The first phase functional has been normalised to its maximum value.

As seen, the validity of the strategy followed in reducing the complexity of the synthesis problem is confirmed. The larger effort is made during the first phase wherein the approximation introduced reduces significantly the computational complexity. On the other

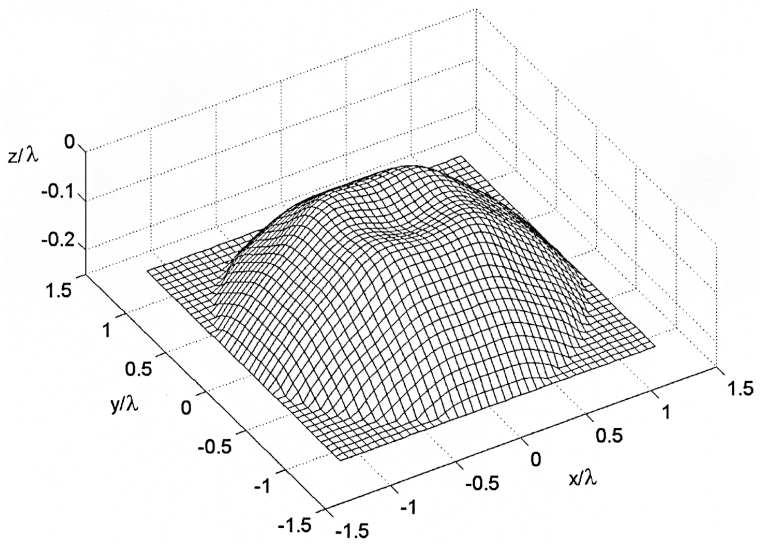

Figure 4. Synthesized subreflector geometry.

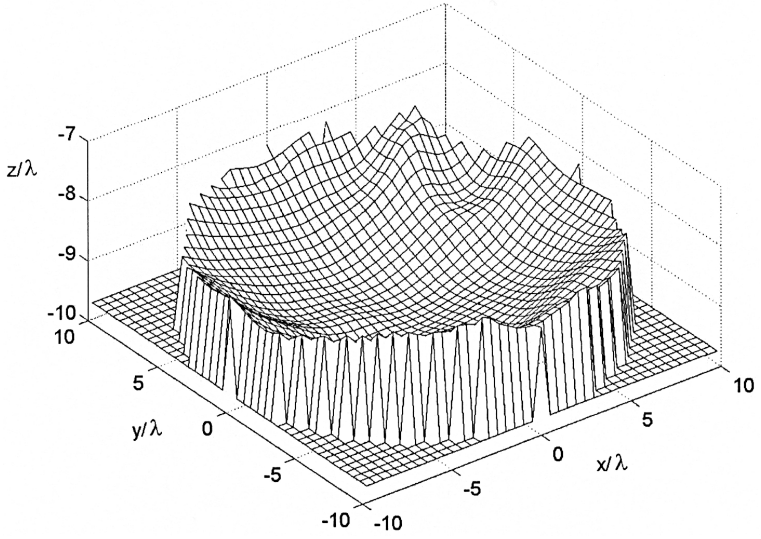

Figure 5. Main reflector geometry synthesized during the first phase.

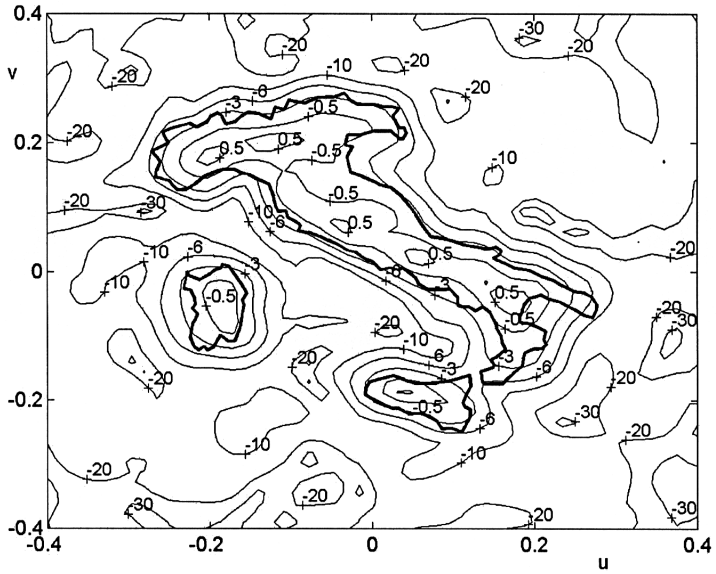

Figure 6. Copolar component synthesized during the second phase.

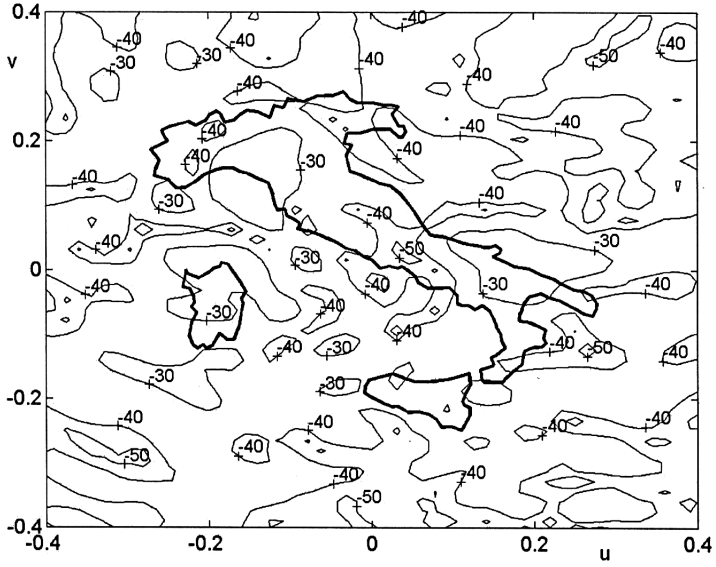

Figure 7. Crosspolar component synthesized during the second phase.

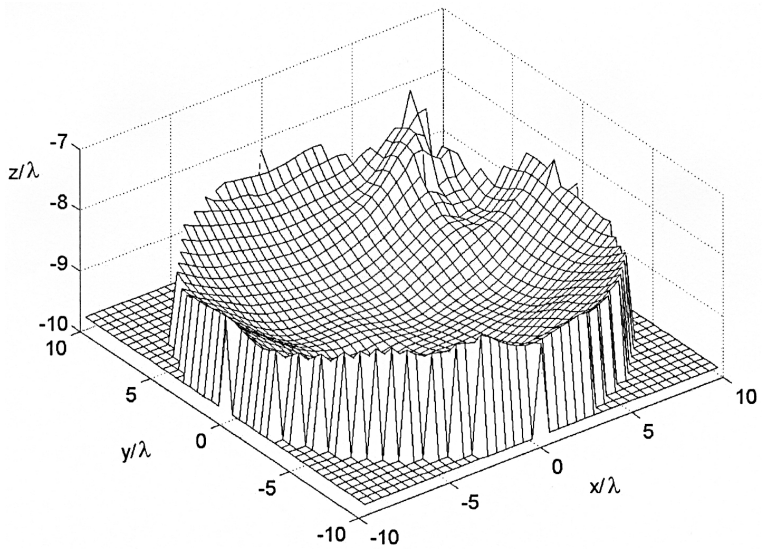

Figure 8. Final main reflector geometry obtained during the second phase.

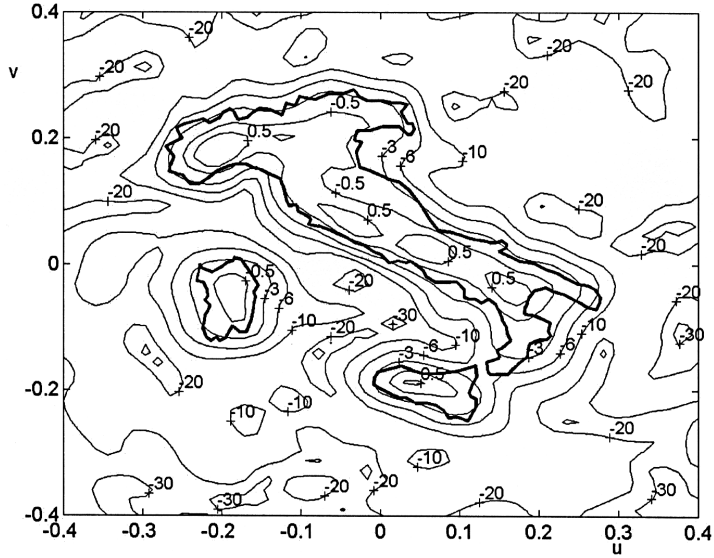

Figure 9. Copolar component of the synthesized antenna evaluated by PO analysis of both reflectors.

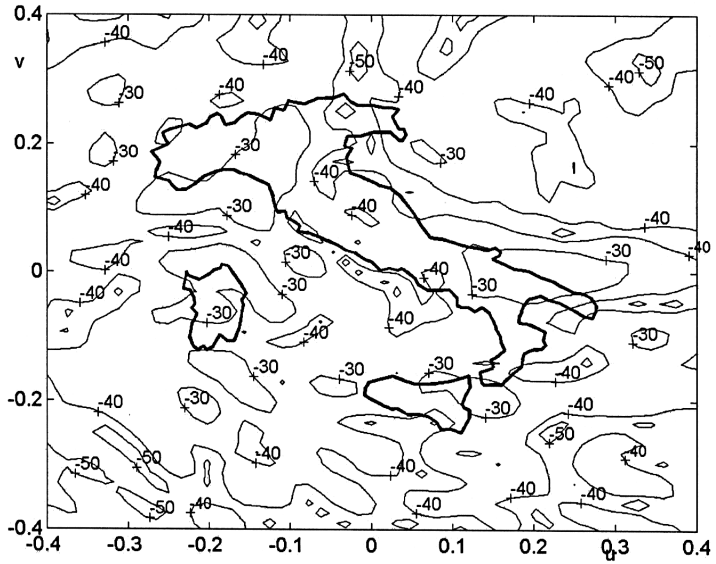

Figure 10. Crosspolar component of the synthesized antenna evaluated by PO analysis of both reflectors.

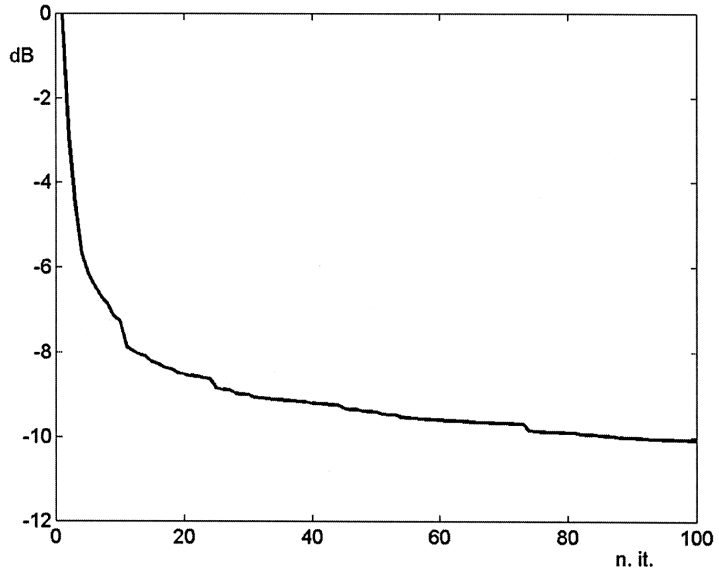

Figure 11. Objective functional decrease during the first phase.

Table 1. Coordinates and excitation coefficients of the elementary radiators.

Feed N	x/λ	y/λ	Amplitude (dB)	Phase (deg)
1	$-.5$	0	-7.6	33
2	0	$-.5$	0	38
3	0	0	-8.8	238
4	0	.5	-7.9	174
5	.5	0	-1.3	-9

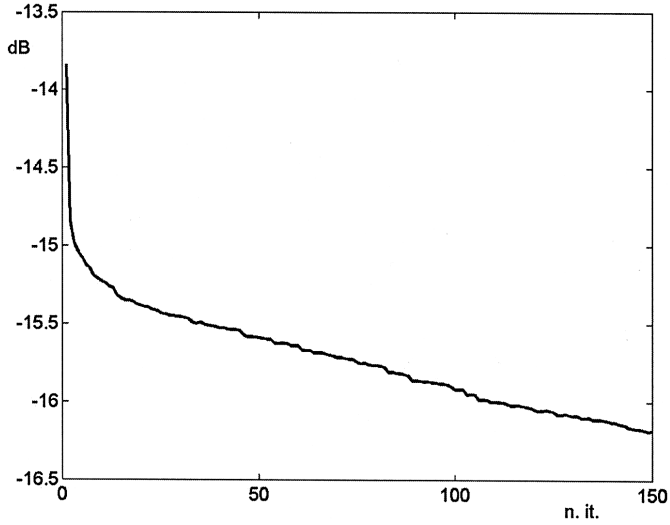

Figure 12. Objective functional decrease during the second phase.

side, as Figs. 9 and 10 show, these approximations are effectively compensated in the second stage of the synthesis procedure.

6. CONCLUSIONS

A new shaped dual-reflector power synthesis technique has been presented. The approach allows to find the main and sub-reflector surface and the excitation coefficients of the primary feed array matching at best the far-field power pattern specifications expressed (in a flexible way) by co-polar and cross-polar squared amplitude upper and lower bounds.

The approach is based on the optimisation of a suitable objective functional, accounting also for regularising terms.

In a first phase, an approximate FFT based model reduces the computational effort to finding the subreflector geometry and a first guess of the main reflector shape. Then, in the second phase, applying the PO and AM technique for the sub-reflector and the main reflector, respectively, the final main reflector surface and the excitation coefficients of the primary feed array are found.

The main advantage of the technique resides in the fact that the main step toward the solution is provided by the first phase wherein the approximations introduced allow using only computational inexpensive operators. The second phase is then needed only to correct for the first phase approximations and, despite the more accurate operators involved, can be effectively performed since it considers a single reflector synthesis problem and a "good" reflector starting guess provided by the first phase of the procedure.

Although, for the sake of numerical effectiveness, the presented approach exploits the AM for the main reflector analysis, it can be straightforwardly extended to the case of PO analysis and to the case of non-planar primary feed array and/or non-uniformly distributed elementary radiators.

Further improvements could be also obtained by exploiting, f.i., the reflector surface and contour representations introduced in [6].

As a concluding remark it is noted that, as proved in [14] in the case of single reflector array fed antennas, the degrees of freedom of the radiating structure can be better exploited if a Global Optimisation technique is considered.

As a consequence, the proposed strategy, that significantly reduces the computational complexity, represents a first step of practical interest toward a hybrid synthesis algorithm.

APPENDIX A.

Concerning eq. (8), let us denote with P and P' two points on the unshaped and deformed reflector, respectively, reflecting the incident ray to the same aperture point A.

The optical path (from a given point O) difference is given by $\delta l = \beta(\overline{PO} + \overline{PA} - (\overline{P'O} + \overline{P'A}))$. At the first order we have:

$$\overline{PA} - \overline{P'A} = (P' - P) \cdot \frac{A - P}{\overline{AP}} \tag{A1}$$

$$\overline{PO} - \overline{P'O} = (P' - P) \cdot \frac{O - P}{\overline{OP}} \tag{A2}$$

so that, applying the law of reflection, we have

$$\begin{aligned}\delta l &= \beta(P'-P)\cdot\left(\frac{A-P}{\overline{AP}}+\frac{O-P}{\overline{OP}}\right)\\ &= \beta(P'-P)\cdot\hat{i}_n 2\cos\alpha = 2\beta\chi\cos\alpha\end{aligned} \tag{A3}$$

being χ the normal component of the deformation $\overline{P'P}$ and α the angle between the reflected ray and $\hat{i}_n$.

APPENDIX B.

Concerning eq. (9a), let us consider a reflection point P and a sphere centered at O. Furthermore, let us denote with α_0 the angle between the normal to the reflector at P, say $\hat{i}_n$, and the line OP, with α_1 and α_2 the minimum and maximum angle between $\hat{i}_n$ and the rays stemming from P and tangent to the sphere and with $2\alpha_S$ the angle subtended by the sphere as seen from P. Assuming a very large reflector curvature, the shift of the reflection point can be neglected and the maximum optical path difference corresponding to a source of rays located at P_S inside the sphere, taking into account eq. (A3), is given by:

$$\max_{P_S}(\delta l_2)-\min_{P_S}(\delta l_2) = 2\beta\chi(\cos\alpha_1-\cos\alpha_2) = 4\beta\chi\sin(\alpha_0)\sin(\alpha_S) \tag{B1}$$

since $\alpha_2-\alpha_1=2\alpha_S$ and $\alpha_2+\alpha_1=2\alpha_0$.

APPENDIX C.

In the practical implementation of the proposed synthesis technique, the unknowns s_1 and s_2 have been represented as:

$$\begin{aligned}s_1(\xi_1,\eta_1) &= \sum_{n=0}^{N_1}\sum_{m=0}^{N_1-n} e'_{nm}T_n(\xi_1)T_m(\eta_1)\\ &= \sum_{k=1}^{V_1} b_{1k}U_k(\xi_1,\eta_1) = \underline{U}_1^T\cdot\underline{b}_1\end{aligned} \tag{C1a}$$

$$\begin{aligned}s_2(\xi_2,\eta_2) &= \sum_{n=0}^{N_2}\sum_{m=0}^{N_2-n} e''_{nm}T_n(\xi_2)T_m(\eta_2)\\ &= \sum_{k=1}^{V_2} b_{2k}U_k(\xi_2,\eta_2) = \underline{U}_2^T\cdot\underline{b}_2\end{aligned} \tag{C1b}$$

where $T_i(x)$ is the Tchebytchev polynomial of i-th degree, N_1, $V_1 = (N_1 + 2)(N_1 + 1)/2$ and N_2, $V_2 = (N_2 + 2)(N_2 + 1)/2$ are the maximum degree of the polynomials and the number of coefficients involved in the representation of s_1 and s_2, respectively, $U_{k(n,m)}(\xi, \eta) = T_n(\xi)T_m(\eta)$, $k(n,m)$ being a one to one correspondence mapping the couple (n,m) onto the index k, $\underline{U}_1 = (U_1, \ldots, U_{V_1})^T$, $\underline{U}_2 = (U_1, \ldots, U_{V_2})^T$, $\underline{b}_1 = (b_{1,1}, \ldots, b_{1,V_1})$ and $\underline{b}_2 = (b_{2,1}, \ldots, b_{2,V_2})$.

From eq. (20), the copolar and crosspolar far-field components are then given by:

$$\begin{aligned}(E_{co}(u_2,v_2), E_{cr}(u_2,v_2)) &= (\mathcal{U}_{co}(\underline{b}_1,\underline{b}_2,\underline{F}_{a0}), \mathcal{U}_{cr}(\underline{b}_1,\underline{b}_2,\underline{F}_{a0})) \\ &= \mathcal{U}(\underline{b}_1,\underline{b}_2,\underline{F}_{a0}) \\ &= \underline{\underline{Q}} \cdot \mathcal{F}^{-1}\Big\{ P_{\Sigma_2} e^{-j2\pi l_{20}} e^{-j2\pi \underline{U}_2^T \cdot \underline{b}_2} \\ &\quad \cdot \mathcal{F}^{-1}\left[P_{\Sigma_{e1}} e^{-j2\pi l_{10}} e^{-j2\pi \underline{U}_1^T \cdot \underline{b}_1} (\mathcal{F}(P_{w_s} \underline{F}_{a0})) \right] \Big\} \end{aligned} \quad \text{(C2)}$$

where the operator $\mathcal{U}$ expresses the functional dependence between the radiated pattern and the unknown.

The first step of the synthesis procedure finds $\underline{b}_1$, $\underline{b}_2$, and $\underline{F}_{a0}$ to meet the design specifications in an approximate mathematical framework by optimising the objective functional:

$$\begin{aligned}&\Phi_1(\underline{b}_1,\underline{b}_2,\underline{F}_{a0}) \\ &= \left\| |\mathcal{U}_{co}(\underline{b}_1,\underline{b}_2,\underline{F}_{a0})|^2 - \mathcal{P}_{\boldsymbol{Y}_{co}} |\mathcal{U}_{co}(\underline{b}_1,\underline{b}_2,\underline{F}_{a0})|^2 \right\|_{w_{co}}^2 \\ &\quad + \left\| |\mathcal{U}_{cr}(\underline{b}_1,\underline{b}_2,\underline{F}_{a0})|^2 - \mathcal{P}_{\boldsymbol{Y}_{cr}} |\mathcal{U}_{co}(\underline{b}_1,\underline{b}_2,\underline{F}_{a0})|^2 \right\|_{w_{cr}}^2 \\ &\quad + \gamma_1 \left\| P_{\Sigma_1} |\nabla_t (l_{10} + \underline{U}_1^T \cdot \underline{b}_1)|^2 - P_{\Sigma_1} \mathcal{P}_{\mathbf{S}_\infty} |\nabla_t (l_{10} + \underline{U}_1^T \cdot \underline{b}_1)|^2 \right\|_1^2 \\ &\quad + \gamma_2 \left\| P_{\Sigma_2} |\nabla_t (l_{20} + \underline{U}_2^T \cdot \underline{b}_2)|^2 - P_{\Sigma_2} \mathcal{P}_{\mathbf{S}_\infty} |\nabla_t (l_{20} + \underline{U}_2^T \cdot \underline{b}_2)|^2 \right\|_1^2 \\ &\quad + \gamma_3 \left\| (1 - P_{\Sigma_{e1}}) \mathcal{F}(P_{w_s} |\underline{F}_{a0}|^2) \right\|_1^2 \end{aligned} \quad \text{(C3)}$$

The minimisation of the functional (C3) can be accomplished by following the general iterative procedure introduced in [12]. In particular, defining:

$$\begin{aligned}&\Phi_2(\underline{b}_1,\underline{b}_2,\underline{F}_{a0},\delta_{co},\delta_{cr},\delta_1,\delta_2) \\ &= \left\| |\mathcal{U}_{co}(\underline{b}_1,\underline{b}_2,\underline{F}_{a0})|^2 - \delta_{co} \right\|_{w_{co}}^2 \\ &\quad + \left\| |\mathcal{U}_{cr}(\underline{b}_1,\underline{b}_2,\underline{F}_{a0})|^2 - \delta_{cr} \right\|_{w_{cr}}^2 \end{aligned}$$

$$
\begin{aligned}
&+\gamma_1 \left\| P_{\Sigma_1} |\nabla_t (l_{10} + \underline{U}_1^T \cdot \underline{b}_1)|^2 - \delta_1 \right\|_1^2 \\
&+\gamma_2 \left\| P_{\Sigma_2} |\nabla_t (l_{20} + \underline{U}_2^T \cdot \underline{b}_2)|^2 - \delta_2 \right\|_1^2 \\
&+\gamma_3 \left\| (1 - P_{\Sigma_{e1}}) \mathcal{F}(|\underline{F}_{a0}|^2) \right\|_1^2
\end{aligned} \tag{C4}
$$

the n-th step consists of the following substeps:

$$
\begin{cases}
\delta_{co}^{(n)} = \mathcal{P}_{\mathbf{Y}_{co}} |\mathcal{U}_{co}(\underline{b}_1^{(n)}, \underline{b}_2^{(n)}, \underline{F}_{a0}^{(n)})|^2 \\
\delta_{cr}^{(n)} = \mathcal{P}_{\mathbf{Y}_{cr}} |\mathcal{U}_{cr}(\underline{b}_1^{(n)}, \underline{b}_2^{(n)}, \underline{F}_{a0}^{(n)})|^2 \\
\delta_1^{(n)} = \mathcal{P}_{S_\infty} P_{\Sigma_1} |\nabla_t (l_{10} + \underline{U}_1^T \cdot \underline{b}_1^{(n)})|^2 \\
\delta_2^{(n)} = \mathcal{P}_{S_\infty} P_{\Sigma_2} |\nabla_t (l_{20} + \underline{U}_2^T \cdot \underline{b}_2^{(n)})|^2
\end{cases} \tag{C5a}
$$

$$
\begin{aligned}
\underline{F}_{a0}^{(n+1)} :\ & \Phi_2(\underline{b}_1^{(n)}, \underline{b}_2^{(n)}, \underline{F}_{a0}^{(n+1)}, \delta_{co}^{(n)}, \delta_{cr}^{(n)}, \delta_1^{(n)}, \delta_2^{(n)}) \\
&= \min_{\underline{w} \in \mathbf{L}_2(\Xi) \times \mathbf{L}_2(\Xi)} \Phi_2(\underline{b}_1^{(n)}, \underline{b}_2^{(n)}, \underline{w}, \delta_{co}^{(n)}, \delta_{cr}^{(n)}, \delta_1^{(n)}, \delta_2^{(n)})
\end{aligned} \tag{C5b}
$$

$$
\begin{aligned}
\underline{b}_1^{(n+1)} :\ & \Phi_2(\underline{b}_1^{(n+1)}, \underline{b}_2^{(n)}, \underline{F}_{a0}^{(n+1)}, \delta_{co}^{(n)}, \delta_{cr}^{(n)}, \delta_1^{(n)}, \delta_2^{(n)}) \\
&= \min_{\underline{w} \in \boldsymbol{C}^{V_1}} \Phi_2(\underline{w}, \underline{b}_2^{(n)}, \underline{F}_{a0}^{(n+1)}, \delta_{co}^{(n)}, \delta_{cr}^{(n)}, \delta_1^{(n)}, \delta_2^{(n)})
\end{aligned} \tag{C5c}
$$

$$
\begin{aligned}
\underline{b}_2^{(n+1)} :\ & \Phi_2(\underline{b}_1^{(n+1)}, \underline{b}_2^{(n+1)}, \underline{F}_{a0}^{(n+1)}, \delta_{co}^{(n)}, \delta_{cr}^{(n)}, \delta_1^{(n)}, \delta_2^{(n)}) \\
&= \min_{\underline{w} \in \boldsymbol{C}^{V_2}} \Phi_2(\underline{b}_1^{(n+1)}, \underline{w}, \underline{F}_{a0}^{(n+1)}, \delta_{co}^{(n)}, \delta_{cr}^{(n)}, \delta_1^{(n)}, \delta_2^{(n)})
\end{aligned} \tag{C5d}
$$

where $\mathbf{C}^N$ is the set of the N-ple of complex numbers.

Now the following comments are of interest.

(i) New additional projections onto $\mathbf{Y}_{co}$, $\mathbf{Y}_{cr}$ could be inserted between steps (C5b) and (C5c) thus updating $\delta_{co}^{(n)}$ and $\delta_{co}^{(n)}$. Analogously, additional projections onto $\mathbf{Y}_{co}$, $\mathbf{Y}_{cr}$ and $\mathbf{S}_\infty$ could be inserted between steps (C5c) and (C5d) thus updating the values of $\delta_{co}^{(n)}$, $\delta_{co}^{(n)}$ and s_1 [12]. This could increase the convergence rate.

(ii) Development of step (C5b) is essentially equivalent to solve a fixed reflectors synthesis problem. Analogously, step (C5c) and (C5d) are equivalent to solve a double reflector synthesis problem with a fixed reflector surface and a fixed primary excitation.

(iii) According to [12], it is not necessary to attain the minimum of Φ_2 during steps (C5b)–(C5d) being only necessary to reduce the values of the functional.

Once the values of $\underline{b}_1$ and $\underline{b}_2$ are obtained, say $\underline{b}_{10}$ and $\underline{b}_{20}$, the corresponding reflector and subreflector shapes can be evaluated as $g_1 = \mathcal{W}(\underline{U}_1^T \cdot \underline{b}_{10})$ and $g_2 = \mathcal{W}(\underline{U}_2^T \cdot \underline{b}_{20})$.

As a consequence, by expressing the functional dependence between the radiated pattern and the actual unknowns $\underline{C}$ and $\underline{b}_1$ by means of the operator $\mathcal{V}$, eq. (21) can be reassessed as:

$$\begin{aligned}
&(E_{co}, E_{cr}) \\
&\quad = (\mathcal{V}_{co}(\underline{b}_1, \underline{b}_2, \underline{C}), \mathcal{V}_{cr}(\underline{b}_1, \underline{b}_2, \underline{C})) \\
&\quad = \mathcal{V}(\underline{b}_1, \underline{b}_2, \underline{C}) \\
&\quad = \underline{\underline{Q}} \cdot \mathcal{F}^{-1}\Bigg\{ P_{\Sigma_2} \hat{i}_{z2} \times \Bigg[\iint_{\Sigma_1} e^{-j\beta(R_1+d)} \frac{\Delta}{R_1} \underline{\underline{R}} \\
&\qquad \cdot (\underline{\underline{I}} - \hat{R}_1 \hat{R}_1) \left[\frac{\partial \mathcal{W}(\mathcal{U}_1^T \cdot \underline{b}_1)}{\partial \xi_1 \partial \eta_1} \right] 2\hat{i}_{n_1} \times \sum_{n=1}^{N_F} C_n \underline{H}_{in} d\xi_1 d\eta_1 \Bigg] \times \hat{i}_{z2} \Bigg\} \\
&\quad = \underline{\underline{Q}} \sum_{n=1}^{N_F} \mathcal{F}^{-1} \left[e^{-j2\pi l_{20}} e^{-j2\pi s_2} \underline{\psi}_n \right]
\end{aligned} \tag{C6}$$

where the functions $\underline{\psi}_n$, $n = 1, \ldots, N_F$, represent the contribution of the n-th elementary radiator of the feeding system to $\underline{F}_{a2}$ (see eq. (13)).

In the second stage of the synthesis procedure the subreflector surface is assumed unchanged and the relationship (C6) is exploited with $\underline{b}_1 = \underline{b}_{10}$.

Accordingly, the final reflector shape and feeding excitation is attained by optimising the functional:

$$\begin{aligned}
&\Psi_1(\underline{b}_2, \underline{C}) \\
&\quad = \left\| \mathcal{V}_{co}(\underline{b}_{10}, \underline{b}_2, \underline{C})|^2 - \mathcal{P}_{\boldsymbol{Y}_{co}} |\mathcal{V}_{co}(\underline{b}_{10}, \underline{b}_2, \underline{C})|^2 \right\|_{w_{co}}^2 \\
&\qquad + \left\| |\mathcal{V}_{cr}(\underline{b}_{10}, \underline{b}_2, \underline{C})|^2 - \mathcal{P}_{\boldsymbol{Y}_{cr}} |\mathcal{V}_{cr}(\underline{b}_{10}, \underline{b}_2, \underline{C})|^2 \right\|_{w_{cr}}^2 \\
&\qquad + \gamma_1 \left\| P_{\Sigma_2} |\nabla_t (l_{20} + \underline{U}_2^T \cdot \underline{b}_2)|^2 - P_{\Sigma_2} \mathcal{P}_{\boldsymbol{S}_\infty} |\nabla_t (l_{20} + \underline{U}_2^T \cdot \underline{b}_2)|^2 \right\|_1^2 \\
&\qquad + \gamma_2 \left\| (1 - P_\Theta) |\underline{H}_i(\underline{C})|^2 \right\|_1^2
\end{aligned} \tag{C7}$$

Considerations analogous to the ones concerning the minimisation of Φ_1 can be repeated for the optimisation of Ψ_1.

In particular, defining:

$$\Psi_2(\underline{b}_2, \underline{C}, \delta_{co}, \delta_{cr}, \delta) \;=\; \left\| |\mathcal{V}_{co}(\underline{b}_{10}, \underline{b}_2, \underline{C})|^2 - \delta_{co} \right\|_{w_{co}}^2$$

$$+\left\|\left|\mathcal{V}_{cr}(\underline{b}_{10},\underline{b}_2,\underline{C})\right|^2-\delta_{cr}\right\|^2_{w_{cr}}$$
$$+\gamma_1\left\|P_{\Sigma_1}\left|\nabla_t(l_{20}+\underline{U}_2^T\cdot\underline{b}_2)\right|^2-\delta\right\|^2_1$$
$$+\gamma_2\left\|(1-P_\Theta)\left|\underline{H}_i(\underline{C})\right|^2\right\|^2_1 \tag{C8}$$

the n-th step of the minimisation algorithm is given by:

$$\begin{cases}\delta_{co}^{(n)}=\mathcal{P}_{\boldsymbol{Y}_{co}}\left|\mathcal{V}_{co}(\underline{b}_{10}^{(n)},\underline{b}_2^{(n)},\underline{C}^{(n)})\right|^2\\ \delta_{cr}^{(n)}=\mathcal{P}_{\boldsymbol{Y}_{cr}}\left|\mathcal{V}_{cr}(\underline{b}_{10}^{(n)},\underline{b}_2^{(n)},\underline{C}^{(n)})\right|^2\\ \delta^{(n)}=\mathcal{P}_{S_\infty}P_{\Sigma_2}\left|\nabla_t(l_{20}+\underline{U}_2^T\cdot\underline{b}_2^{(n)})\right|^2\end{cases} \tag{C9a}$$

$$\underline{C}^{(n+1)}:\ \Psi_2(\underline{b}_2^{(n)},\underline{C}^{(n+1)},\delta_{co}^{(n)},\delta_{cr}^{(n)},\delta^{(n)})$$
$$=\min_{\underline{w}\in\boldsymbol{C}^{N_F}}\Psi_2(\underline{b}_2^{(n)},\underline{w},\delta_{co}^{(n)},\delta_{cr}^{(n)},\delta^{(n)}) \tag{C9b}$$
$$\underline{b}_2^{(n+1)}:\ \Psi_2(\underline{b}_2^{(n+1)},\underline{C}^{(n+1)},\delta_{co}^{(n)},\delta_{cr}^{(n)},\delta^{(n)})$$
$$=\min_{\underline{w}\in\boldsymbol{C}^{V_2}}\Psi_2(\underline{w},\underline{C}^{(n+1)},\delta_{co}^{(n)},\delta_{cr}^{(n)},\delta^{(n)}) \tag{C9c}$$

The same considerations made at points (i)–(iii) above and concerning the iterative procedure (C5) apply also to the iterative procedure (C9). It must be noted that, now, step (C9c) is particularly heavy since Ψ_2 depends on $\underline{b}_2$ not only through the exponential term in eq. (C6) but also, in a complex way, through the functions $\underline{\psi}_n$. However, as previously discussed, these functions are weakly dependent on the main reflector surface, hence on $\underline{b}_2$, so that, for small variations of the reflector shape, they can be held constant. Accordingly, by neglecting in the step (C9c) the dependence of $\underline{\psi}_n$ on $\underline{b}_2$, an approximate procedure for the minimisation of Ψ_2 can be devised, with a very significant saving of computer time [13]. However, it may happen that the above approximation cannot be pursued for many iterations. In this case the functions $\underline{\psi}_n$ (and thus the reference reflector to which they are related and the corresponding optical path l_{20}) should be updated to make the above approximate procedure still reliable.

Usually, only at the beginning of the procedure the update is required frequently. In fact, when the iterations have already proceeded, only small variations of the main reflector geometry are involved and the updating can be performed once or, in many cases, can be avoided at all.

REFERENCES

1. Descardeci, J. C. and C. G. Parini, "Trireflector compact antenna test range," *IEE Proc. Microw. Antenna Propag.*, Vol. 144, No. 5, 305–310, October 1997.
2. Kildal, P. S., "Synthesis and analysis of a dual-reflector feed for the radiotelescope in Nancy," *IEE Proc. Microw. Antennas Propag.*, Vol. 144, No. 5, 289–296, October 1997.
3. Kildal, P. S., L. Baker, and T. Hagfors, "The Arecibo upgrading: electrical design and expected performance of the dual-reflector feed system," *Special Issue of Proc. IEEE*, Vol. 82, No. 5, 714–724, 1994.
4. Viskum, H. H., K. Pontoppidan, P. J. B. Clarricoats, and G. A. E. Crone, "Coverage flexibility by means of a reconfigurable subreflector," *IEEE AP-S Symposium Digest*, Montreal, Canada, 1378–1381, 1997.
5. Viskum, H. H., S. B. Sorensen, and K. Pontoppidan, "A dual reflector system with a reconformable subreflector," *IEEE Antennas and Propagation Society International Symposium*, Vol. 2, 840–843, 1998.
6. Duan, D. W. and Y. Rahmat-Samii, "A generalized diffraction synthesis technique for high performance reflector antennas," *IEEE Trans. Antenn. Propagat.*, Vol. 43, No. 1, 27–40, January 1995.
7. Westcott, B. S., F. A. Stevens, and F. Brickell, "GO synthesis of offset dual reflectors," *IEE Proc. Part. H*, Vol. 128, No. 1, 11–18, February 1981.
8. Cherrette, A. R., S. W. Lee, and R. J. Acosta, "A method for producing a shaped contour radiation pattern using a single shaped reflector and a single feed," *IEEE Trans. Antenn. Propagat.*, Vol. 37, No. 6, 698–706, June 1989.
9. Bergmann, J., R. C. Brown, P. J. B. Clarricoats, and H. Zhou, "Synthesis of shaped-beam reflector antenna patterns," *IEE Proc., Part. H*, Vol. 135, No. 1, 48–53, February 1988.
10. Hay, S. G., "Dual-shaped-reflector directivity pattern synthesis using the successive projections method," *IEE Proc. Microw. Antennas Propagat.*, Vol. 146, No. 2, 119–124, April 1999.
11. Westcott, B. S. and A. A. Zaporozhets, "Dual-reflector synthesis based on analytical gradient-iteration procedures," *IEE Proc. Microw. Antennas Propagat.*, Vol. 142, No. 2, 129–135, April 1995.
12. Bucci, O. M., G. D'Elia, G. Mazzarella, and G. Panariello, "Antenna pattern synthesis: a new general approach," *Proc. of*

IEEE, Vol. 82, No. 3, 358–371, March 1994.

13. Bucci, O. M., G. D'Elia, and G. Romito, "Synthesis technique for scanning and/or reconfigurable beam reflector antennas with phase-only control," *IEE Proc. Part. H*, Vol. 13, No. 5, 402–412, October 1996.
14. Bucci, O. M., A. Capozzoli, and G. D'Elia, "A global optimization technique in the synthesis of reflector antennas," *17th Annual Review of Progress in Applied Computational Electromagnetics*, Monterey, CA, March 19–23, 2001.
15. Hoferer, R. A. and Y. Rahmat-Samii, "A GO-subreflector implementation methodology using a Fourier-Jacobi surface expansion," *Proceedings of the IEEE Antennas and Propagation Society*, Vol. 4, 2328–2331, 1999.
16. Yaghjian, A. D., "Equivalence of surface current and aperture field integration for reflector antennas," *IEEE Transaction on Antennas and Propagat.*, Vol. AP-32, No. 12, 1355–1358, Dec. 1984.
17. Born, M. and E. Wolf, *Principles of Optics*, 7th edition, Cambridge University Press, 1999.
18. Westcott, B. S., *Shaped Reflectors Antenna Design*, London Research Studies Press Ltd., 1983.
19. Luenberger, D. G., *Linear and Non Linear Programming*, Academic Press London, 1984.